Progress in Nuclear Energy 99 (2017) 110–118

Contents lists available at ScienceDirect

Progress in Nuclear Energy

journal homepage: www.elsevier.com/locate/pnucene

# Mechanical, electronic and thermodynamic properties of hexagonal and orthorhombic $U_2Mo$: A first-principle calculation

Ke Chen [a, c], Xiaofeng Tian [a, *], You Yu [b], Zhenjiang You [d], Liangquan Ge [a], Changlun Chen [c]

[a] The College of Nuclear Technology and Automation Engineering, Chengdu University of Technology, Chengdu, 610059, China
[b] College of Optoelectronic Technology, Chengdu University of Information Technology, Chengdu, 610225, China
[c] Key Lab of New Thin Film Solar Cells, Institute of Plasma Physics, Chinese Academy of Sciences, Hefei, 230031, China
[d] Australian School of Petroleum, University of Adelaide, SA 5005, Australia

ARTICLE INFO

*Article history:*
Received 15 June 2016
Received in revised form
3 April 2017
Accepted 15 May 2017
Available online 24 May 2017

*Keywords:*
$U_2Mo$
Elastic properties
Phonon dispersion relations
Stress-strain relations
Density functional theory

ABSTRACT

First-principle investigations are presented based on density functional approach to calculate the elastic properties, stress-strain relations, phonon dispersion relations, electronic properties and thermodynamic properties of hexagonal and orthorhombic $U_2Mo$. The calculated energies in the present work suggest that hexagonal structure is more stable than orthorhombic one. The obtained elastic constants and moduli show that both phases of $U_2Mo$ are ductile and elastically stable. Besides, the stress-strain relations and the corresponding theoretical tensile strengths of these two phases exhibit strong anisotropy in selected crystalline directions. The generated phonon dispersion curves without imaginary phonon mode imply these two compounds are dynamically stable. The analyzed results of the electrical properties demonstrate the electronic stability, and the hybridizations between the *f*-states of U and the *d*-states of Mo can be noted from derived band structures and partial densities of states for these two structures. Gibbs free energy and other thermodynamics quantities are also obtained and discussed in this paper.



## 1. Introduction

Uranium is the main component in nuclear fuel. Pure uranium exhibits three allotropic phases: a low-temperature orthorhombic α-phase (space group Cmcm), a high-temperature tetragonal β-phase (space group $P4_2/mmm$) and a higher temperatures body-centered cubic γ-phase (space group $Im\bar{3}m$) (Rechtien and Nelson, 1973). The α-U has a number of disadvantages that make it unacceptable for use as nuclear reactor fuel, such as poor oxidation and corrosion resistance, low hardness and yield strength. One of the effective and useful ways is to make uranium alloyed with other elemental metals (from groups V to VIII). Up to now, several elements such as Mo, Nb, Ti, and Zr have been proved to exhibit high degree of solid solubility in γ-U at high temperature (Tupper et al., 2012). Among them, U-Mo alloys have been regarded as the most prominent candidates because of their more stable irradiation performance compared with other high density uranium alloys and compounds.

Many researchers (Van Thyne and McPherson, 1957; Tangri and Williams, 1961; Craik et al., 1962; Howlett, 1970; Dabush et al., 2002; Burkes et al., 2009; Pedrosa et al., 2015) have carried out metallographic investigations of U-Mo system, and the thermodynamic properties for various U-Mo alloys ((Burkes et al., 2010a, 2010b; Kutty et al., 2012) were also experimentally investigated. It was found that Mo exhibits a high solubility (*ca.*35 *at.*%) in bcc γ-U at high temperature, but below 833 K the equilibrium state becomes a mixture of α-U and the intermetallic compound $U_2Mo$ (Rough and Bauer, 1958). Experimental measurements have already revealed that the synthesized $U_2Mo$ is a $MoSi_2$ type compound having a $C11_b$ structure (space group I4/mmm). The phase transformation from $U_2Mo$ to bcc γ-phase was also observed at 853 K (Kutty et al., 2012). In fact, the $U_2Mo$ compound is a compromise between high fissile material density and stable behavior.

For years, many theoretical results on U-based alloys have been reported (Alonso and Rubiolo, 2007; Landa et al., 2011; Jaroszewicz et al., 2013; Wang et al., 2014; Liu et al., 2015; Losada and Garcés, 2015, 2016). Alonso and Rubiolo (2007) firstly evaluated the thermodynamic functions of U-Mo systems employing the first principle calculations. Landa et al. (2011) studied the ground-state properties of U-Mo solid solutions by density functional theory.

* Corresponding author.
*E-mail address:* txf8378@163.com (X. Tian).

http://dx.doi.org/10.1016/j.pnucene.2017.05.012
0149-1970/

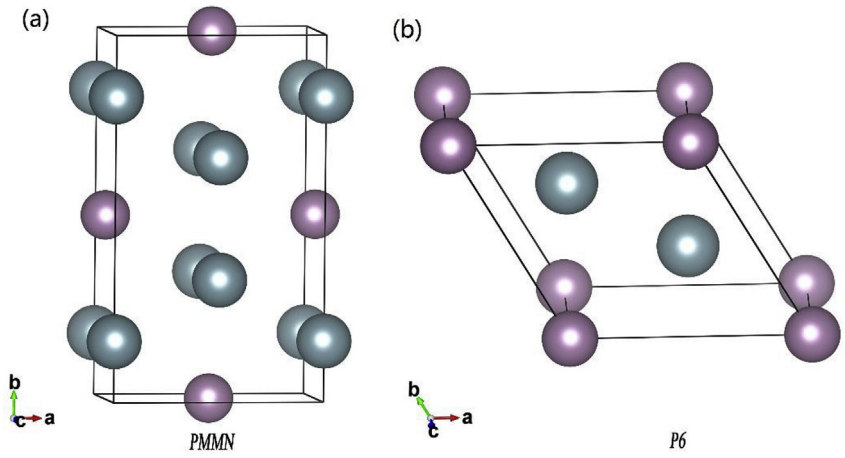


**Fig. 1.** The structure of $U_2Mo$: (a) orthorhombic (Pmmn) phase; (b) hexagonal (P6) phase. The purple and light blue circles are Mo and U atoms, respectively. (For interpretation of the references to colour in this figure legend, the reader is referred to the web version of this article.)

**Table 1**
The optimized structural parameters (lattice constant in Å, the atomic positions).

| | a | b | c | U | Mo | References |
|---|---|---|---|---|---|---|
| Pmmn | 4.831 | 8.315 | 2.720 | (0,0.167,1.0) | (0,0.5,0.5) | Wang et al. (2014) |
| Pmmn | 4.817 | 8.342 | 2.740 | (0,0.167, 1.0) | (0,0.5,0.5) | This work |
| P6 | 4.821 | 4.821 | 2.773 | (0.333, 0.667,0.5) | (0,0,0) | Losada and Garcés (2016) |
| P6 | 4.818 | 4.818 | 2.738 | (0.333, 0.667,0.5) | (0,0,0) | This work |

**Table 2**
Calculated elastic constants (in GPa), bulk modulus B, shear modulus G, B/G, Young's modulus Y and Poission's ratio υ of Pmmn and P6 phase of $U_2Mo$ (all in GPa except for υ).

| | $C_{11}$ | $C_{22}$ | $C_{33}$ | $C_{44}$ | $C_{55}$ | $C_{66}$ | $C_{13}$ | References |
|---|---|---|---|---|---|---|---|---|
| Pmmn | 299 | 293 | 246 | 74 | 73 | 87 | 116 | Wang et al. (2014) |
| Pmmn | 298.37 | 296.33 | 242.19 | 63.34 | 83.66 | 66.74 | 120.96 | This work |
| P6 | 304 | – | 288 | 66 | – | – | 103 | Losada and Garcés (2016) |
| P6 | 272.52 | – | 227.30 | 78.37 | – | – | 104.18 | This work |
| | $C_{12}$ | $C_{23}$ | B | G | G/B | Y | υ | |
| Pmmn | 131 | 133 | 198 | 91 | 0.46 | 238 | 0.30 | Wang et al. (2014) |
| Pmmn | 131.44 | 122.85 | 195.29 | 72.96 | 0.37 | 194.6 | 0.334 | This work |
| P6 | 123 | – | 173 | 81 | 0.47 | 210 | 0.3 | Losada and Garcés (2016) |
| P6 | 112.33 | – | 156.33 | 77.31 | 0.49 | 199.2 | 0.2877 | This work |

Jaroszewicz et al. (2013) calculated the mechanical and thermal properties with a conclusion that $U_2Mo$ of $C11_b$ structure has structural stability. However, the consistent conclusion that I4/mmm structural $U_2Mo$ is a mechanically and dynamically unstable phase has been obtained in recent years (Wang et al., 2014; Liu et al., 2015; Losada and Garcés, 2015). So, searching for a stable phase of $U_2Mo$ attracted many researchers' attention. Wang et al. (2014) found a stable orthorhombic structure of $U_2Mo$ (space group Pmmn) by first principle calculations. More recently, a new ground-state of hexagonal $U_2Mo$ (space group P6) was also found (Losada and Garcés, 2015). To date, there is no systematic study of mechanical, electronic and thermodynamic properties of these two structures, which are significantly important for experimental synthesis and practical application in the future. Thus, a theoretical predication of structural, mechanical and thermodynamic properties of orthorhombic and hexagonal $U_2Mo$ is urgently needed.

Therefore, in this paper, we employ density-functional theory calculation to investigate the hexagonal and orthorhombic $U_2Mo$. The elastic properties, stress-strain relations, phonon dispersion relations, electrical properties and thermodynamic properties were taken into account and systematically calculated. The paper is organized as follows: Section 2 describes the computational details of this study. In Section 3, the theoretical properties of $U_2Mo$ compound with two different phases are presented and discussed in detail. General conclusions in section 4 finalize the paper.

## 2. Computation method

In the present work, the first-principle calculations were carried out within density-functional theory (DFT), as implemented in Vienna Ab initio Simulation Package (VASP) code (Kresse and Hafner, 1993; Kresse and Furthmüller, 1996a, b). The plane-wave basis set was employed within the framework of the projector augmented wave (PAW) method (Blöchl, 1994; Kresse and Joubert, 1999). GGA calculations were employed using exchange-correlation functional parameterized by Perdew, Burke and Ernzerhof (PBE) (Perdew et al., 1996). The cutoff energy of 500 eV were used in all calculations and the *k*-point meshes in the Brillouin zone (BZ) were sampled by 11 × 11 × 11 for orthorhombic Pmmn structure and 11 × 11 × 13 for hexagonal P6 structure according to Monkhorst-Pack scheme. During structural optimization, the

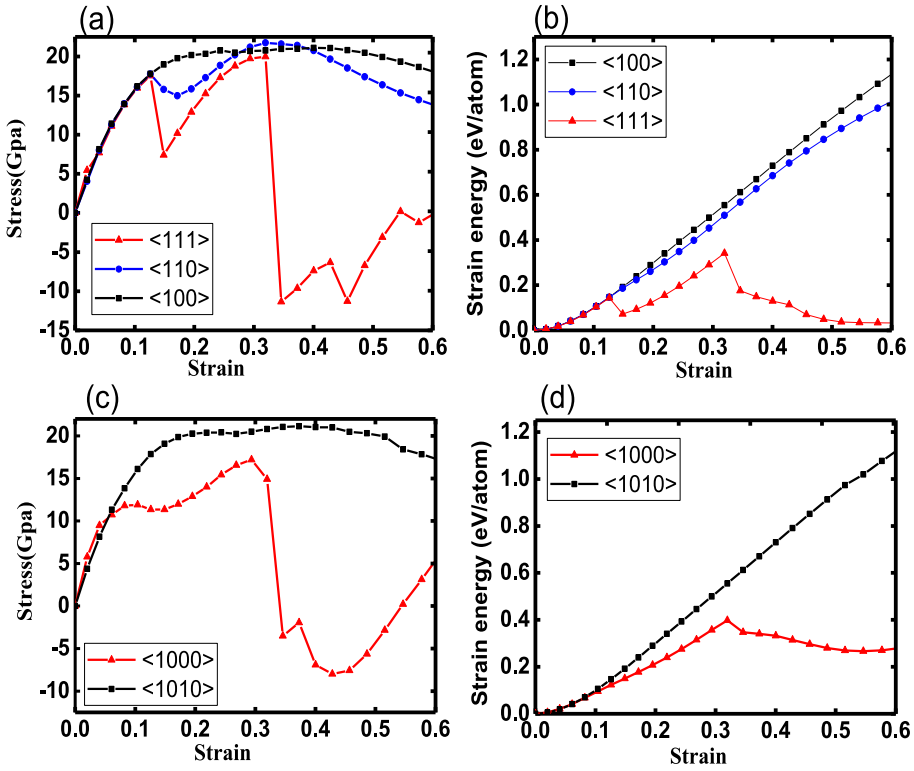


**Fig. 2.** (a) The stress-strain curves of $U_2Mo$ in Pmmn phase; (b) The energy-stress curves of $U_2Mo$ in Pmmn phase; (c) The stress-strain curves of $U_2Mo$ in P6 phase; (d) The energy-stress curves of $U_2Mo$ in P6 phase.

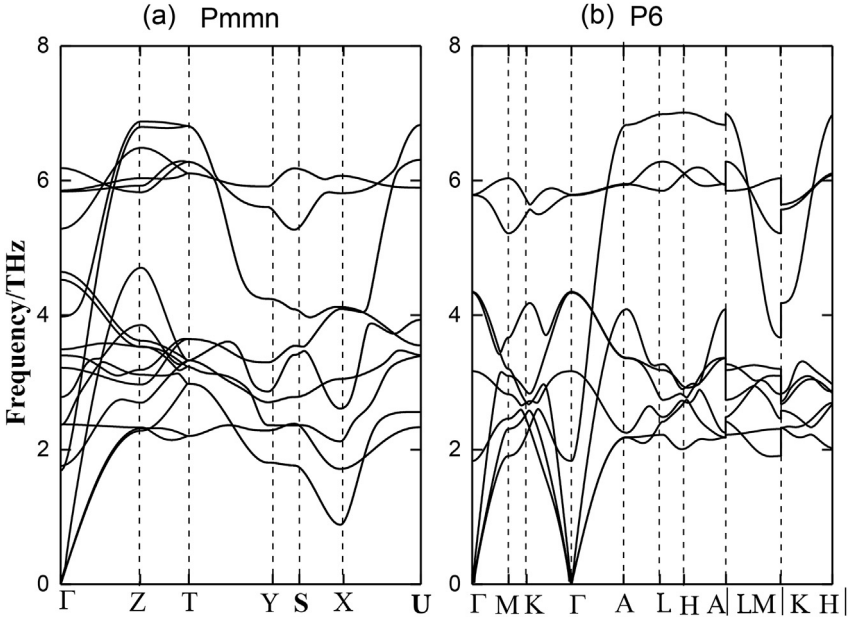


**Fig. 3.** (a) The phonon spectrum of $U_2Mo$ in Pmmn phase; (b) The phonon spectrum of $U_2Mo$ in P6 phase.

convergence tolerance of the energy and force were $1.0 \times 10^{-5}$ eV and $1.0 \times 10^{-3}$ eV Å$^{-1}$ respectively. In the calculations of electrical property, the *k*-mesh sampling was increased to $15 \times 15 \times 15$ for these two structures to get accurate results.

In order to obtain the vibrational thermodynamic properties, we carried out the phonon calculation by the supercells approach (Togo et al., 2008, 2010). Using density functional perturbation theory (DFPT) (Baroni et al., 1987, 2001) implemented in the VASP code, force constants were generated to obtain phonon spectra. The $2 \times 2 \times 2$ supercells were chosen to calculate thermodynamic properties based on Quasi-harmonic approximation (QHA) at ten different volumes for Pmmn phase and eight different volumes for P6 phase.

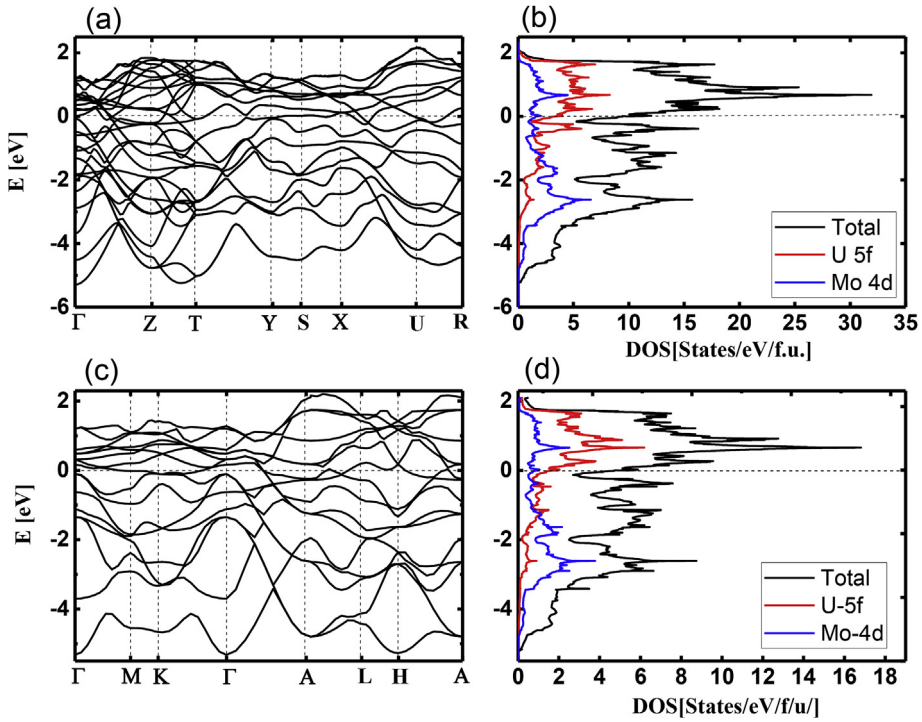


**Fig. 4.** (a) The calculated band structure of $U_2Mo$ in Pmmn phase; (b) The densities of states (DOSs) of $U_2Mo$ in Pmmn phase; (c) The calculated band structure of $U_2Mo$ in P6 phase (d) The densities of states (DOSs) of $U_2Mo$ in P6 phase.

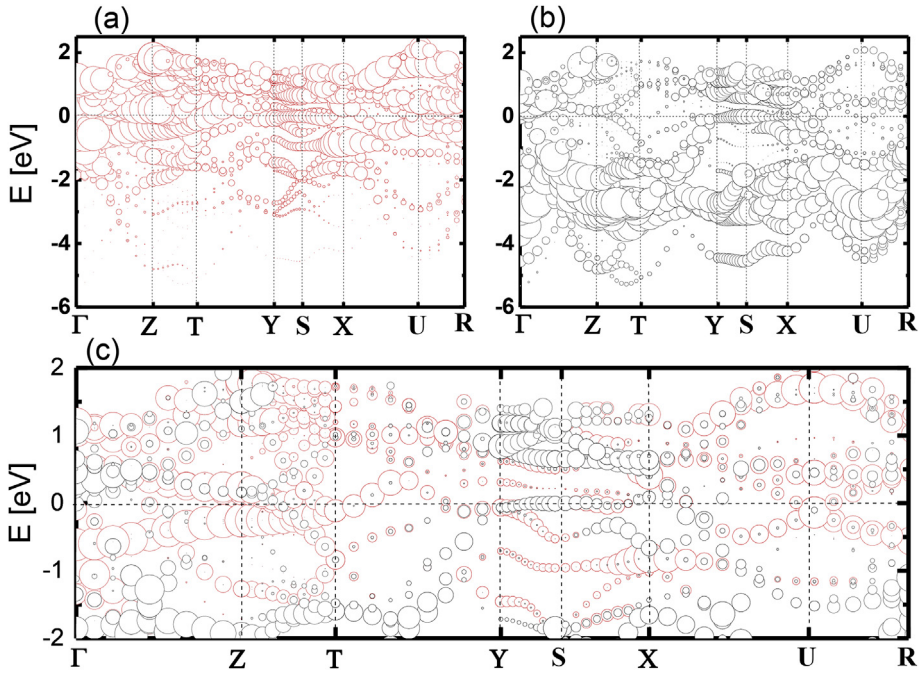


**Fig. 5.** (a) The band structure of *f*-states of U for $U_2Mo$ in Pmmn phase; (b) The band structure of *d*-states of Mo for of $U_2Mo$ in Pmmn phase; (c) The band structure of $U_2Mo$ in Pmmn phase merged U-*f* and Mo-*d* near the Fermi level.

## 3. Results and discussions

For orthorhombic Pmmn structure, as depicted in Fig. 1 (a), the calculated lattice parameters are $a_0 = 4.817$ Å, $b_0 = 8.342$ Å and $c_0 = 2.740$ Å, respectively. The values of lattice parameters are $a = b = 4.818$ Å, $c = 2.738$ Å for hexagonal P6 structure, which is shown in Fig. 1 (b). Our results are consistent with the recent theoretical calculations (Wang et al., 2014; Losada and Garcés, 2016), as listed in Table 1. In addition, the energies at their equilibrium volume were obtained, and the calculated energies elucidated that the energy of hexagonal $U_2Mo$ is lower than that of orthorhombic of $U_2Mo$ by 0.0365mRy, indicating that the P6 phase

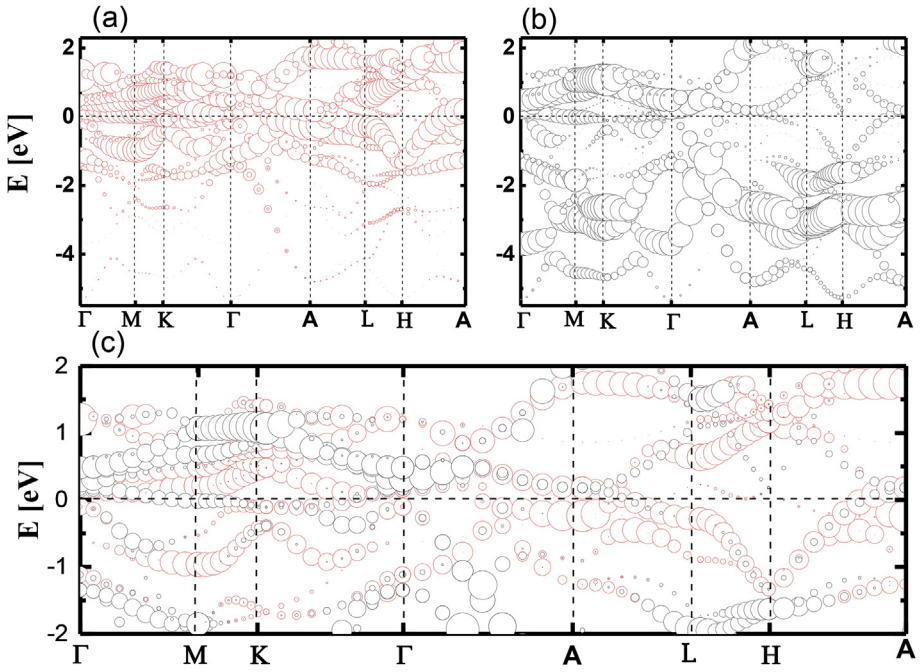


**Fig. 6.** (a) The band structure of *f*-states of U for $U_2Mo$ in P6 phase; (b) The band structure of *d*-states of Mo for $U_2Mo$ in P6 phase; (c) The band structure of $U_2Mo$ in P6 phase merged U-*f* and Mo-*d* near the Fermi level.

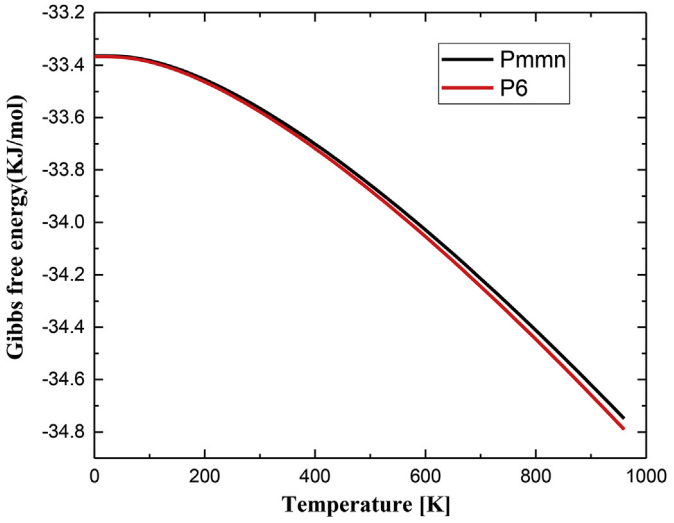


**Fig. 7.** The Gibbs free energies of $U_2Mo$ in Pmmn and P6 phases as a function of temperature.

is more energetically stable than the Pmmn phase.

Elastic constants could describe the elastic deformations of crystals, and elastic properties are related to the mechanical and thermal properties. In this work, five single-crystal elastic constants ($C_{11}$, $C_{12}$, $C_{13}$, $C_{33}$, $C_{44}$) for the hexagonal structure of $U_2Mo$ were selected, whereas nine independent components of the elasticity tensor ($C_{11}$, $C_{22}$, $C_{33}$, $C_{44}$, $C_{55}$, $C_{66}$, $C_{13}$, $C_{12}$, $C_{23}$) for orthorhombic $U_2Mo$ were used. Table 2 presents the computed results for these two structures. As shown in Table 2, the elastic constants of both phases calculated in present work are in good agreement with previous DFT results by Wang et al. (2014) and Losada and Garcés, (2016), validating the reliability of the mechanical results presented in this work. In order to examine the mechanical stability, we refer to the Born-Huang stability criteria (Born and Huang, 1954). For orthorhombic Pmmn phase, the mechanical stability criterion is:

$$C_{11}>0,\ C_{22}>0,\ C_{33}>0,\ C_{44}>0,\ C_{55}>0,\ C_{66}>0,\ C_{11}+C_{22}+C_{33}+2(C_{12}+C_{13}+C_{23})>0,\ C_{11}+C_{22}-2C_{12}>0,\ C_{11}+C_{33}-2C_{13}>0,\ \text{and}\ C_{22}+C_{33}-2C_{23}>0. \quad (1)$$

For phases with hexagonal P6 phase, the criterion is:

$$C_{44}>0,\ C_{66}=\frac{C_{11}-C_{12}}{2}>0,\ C_{11}+C_{12}-\frac{2C_{13}^2}{C_{33}}>0 \quad (2)$$

From Table 2 we can draw a conclusion that all the calculated elastic constants satisfy these conditions, confirming the elastic stability of the both phases.

Bulk and shear modulus values were calculated based on the Voigt-Reuss-Hill (VRH) method (Voigt, 1928; Reuss, 1929; Hill, 1952). The bulk modulus B, shear modulus G, Young's modulus E and Poisson's ratio υ were also obtained. The corresponding results are listed in Table 2. It is well known that the hardness of materials is related to the shear modulus and Young's modulus (Hill, 1952). The higher the shear modulus and Young's modulus are, the higher the hardness is. We note from Table 2 that the hardness of P6 phase is higher than that of Pmmn phase, which can be attributed to the higher shear modulus and Young's modulus of hexagonal $U_2Mo$. What's more, the hardness and the brittleness of the compound are associated with the G/B value (Pugh, 1954). If G/B < 0.5, the compound is ductile and has lower hardness, while G/B > 0.5, the compound is brittle and has a higher hardness. In our work, we can get that the values of G/B for both phases of $U_2Mo$ are lower than 0.5, implying the orthorhombic and hexagonal $U_2Mo$ are ductile.

In order to further investigate the intrinsic mechanical properties, the stress-strain relationships under tensile were calculated. The tensile strengths were performed along the <100>, <110>, <111> directions for orthorhombic Pmmn structure and <1000>,

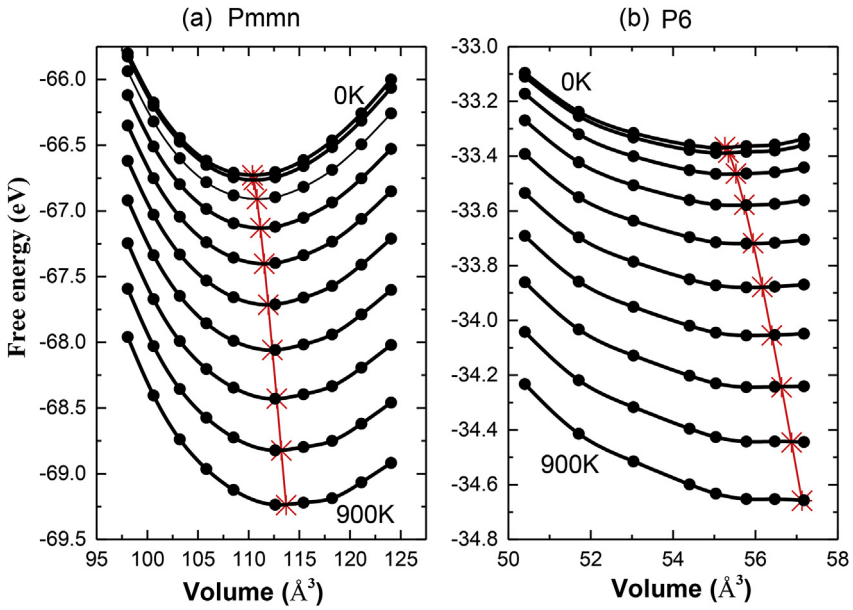


**Fig. 8.** Free energy of $U_2Mo$ as a function of unit cell volume. (a) Pmmn phase; (b) P6 phase.

**Table 3**
The lattice parameters for each temperature (lattice constant in Å).

| T(K) | Pmmn | | | P6 | | |
|---|---|---|---|---|---|---|
| | a | b | c | a | b | c |
| 0 | 4.820 | 8.348 | 2.743 | 4.821 | 4.821 | 2.740 |
| 100 | 4.822 | 8.350 | 2.745 | 4.823 | 4.823 | 2.742 |
| 200 | 4.826 | 8.357 | 2.748 | 4.827 | 4.827 | 2.746 |
| 300 | 4.830 | 8l365 | 2.750 | 4.833 | 4.833 | 2.750 |
| 400 | 4.835 | 8.374 | 2.755 | 4.837 | 4.837 | 2.754 |
| 500 | 4.839 | 8.381 | 2.759 | 4.843 | 4.843 | 2.758 |
| 600 | 4.846 | 8.392 | 2.763 | 4.848 | 4.848 | 2.762 |
| 700 | 4.849 | 8.398 | 2.769 | 4.852 | 4.852 | 2.766 |
| 800 | 4.855 | 8.408 | 2.774 | 4.859 | 4.859 | 2.769 |
| 900 | 4.861 | 8.418 | 2.779 | 4.861 | 4.861 | 2.775 |

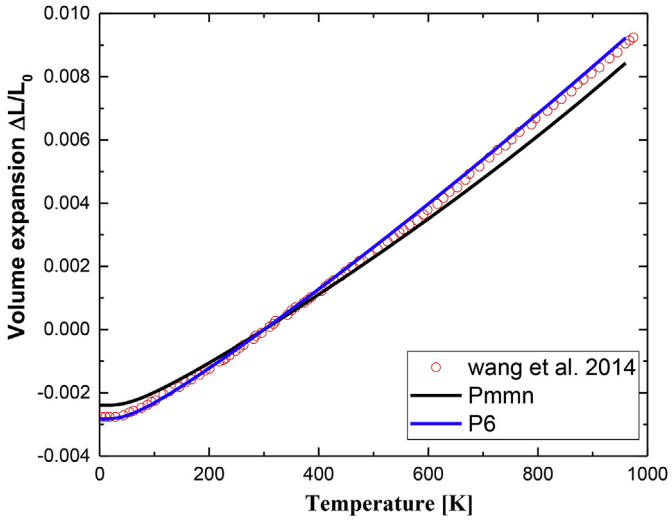


**Fig. 9.** The volume expansion of $U_2Mo$ in Pmmn and P6 phases of as a function of temperature.

<1010> directions for hexagonal P6 structure. The dependence of stress and relative energies on tensile strain is shown in Fig. 2. The ideal strength was considered to be related to the onset of fracture and dislocation nucleation in defect-free materials (Zhang et al., 2007); while we found that the ideal tensile strength of orthorhombic $U_2Mo$ is independent on the tensile directions, and the values are about 18–21 GPa for the three directions. In <100> and <110> directions, the energy increases with the increasing tensile strain but there is a different trend of the relative energy in <111> direction. In this tensile direction, the stress reaches a maximum of 19.8 GPa at a strain of 0.3 and then drops rapidly to a negative stress of −12.1 GPa at a strain of 0.34. It can be found that the maximum of the energy also appears at the strain of 0.3, and then the energy decreases gradually with the tensile strain.

For the hexagonal phase, the tensile ideal strength along <1010> direction is about 21.2 GPa, higher than the value of 14.6 GPa along the <1000> direction. The energy under tensile loading along <1010> direction increases with tensile strain. While in <1000>direction, the stress increase initially with tensile stain and reaches the maximum value of 14.6 GPa at strain of 0.31, then drops rapidly to a minimum of −9.8 GPa at strain of 0.44. The energy in this direction exhibits a maximum at the strain of 0.31, followed by a slow decrease with increasing tensile strain.

To get better understanding of the dynamical stability of the structure, we further calculated the full phonon dispersion curves along major symmetry directions in Brillouin zone using $2 \times 2 \times 2$ supercells. Fig. 3 (a) and (b) show the phonon dispersion curves of orthorhombic and hexagonal $U_2Mo$, respectively. A crystal lattice with $n$ atoms per unit cell has $3n$ branches, hence there are 18 branches for Pmmn phase and 9 branches for P6 phase. For these two structures, there are three acoustic branches and the rest are optical. In our calculations, there are no imaginary frequencies for both structures, suggesting that these two phases of $U_2Mo$ are dynamically stable. This conclusion is in line with the elastic constants analysis.

The electronic structure is of great importance to shed light on some physical properties of materials. In Fig. 4, we give the band structures of $U_2Mo$ along high symmetry points in Brillouin zone, accompanied by the total and partial densities of states. We noted

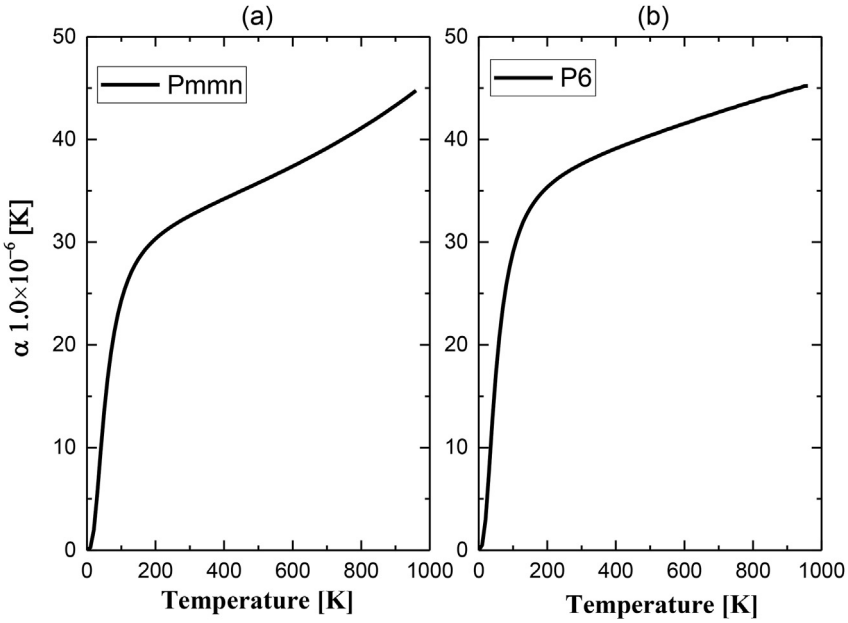


**Fig. 10.** (a) Thermal expansion coefficients of $U_2Mo$ as a function of temperature. (a) Pmmn phase; (b) P6 phase.

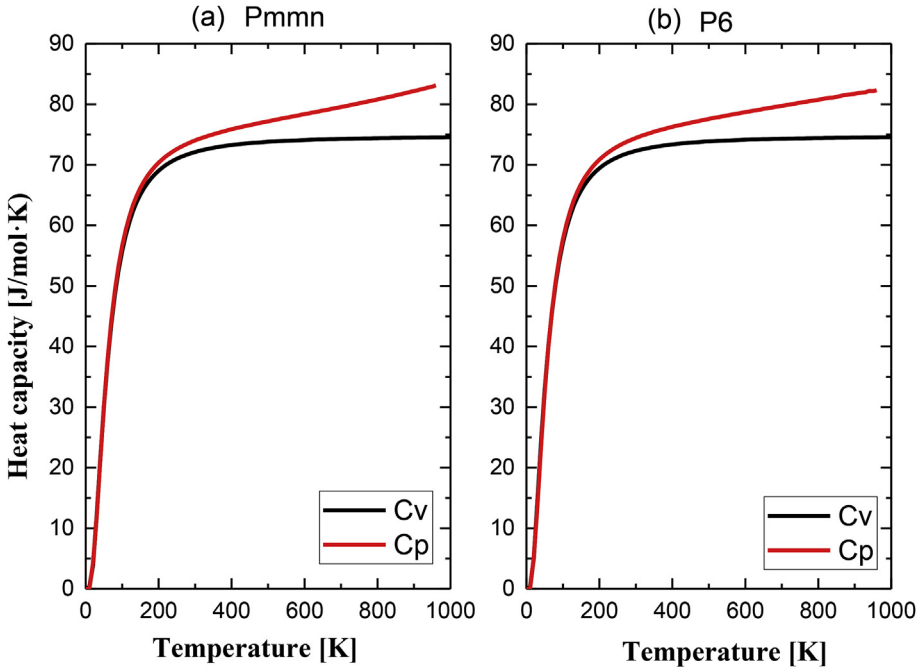


**Fig. 11.** (a) The specific heat capacities of $U_2Mo$ as a function of temperature. (a) Pmmn phase; (b) P6 phase.

that Fermi levels locate near the pseudogaps for the both phases, which implies the electronic stability for the two structures of $U_2Mo$. The total density of states at Fermi level of hexagonal $U_2Mo$ is significantly reduced compared with the orthorhombic phase. Through analysis of partial densities of states, it can be obtained that Mo-4*d* and U-5*f* electrons exhibit relatively stronger hybridization for both phases. To get a clear insight in this hybridization, the band for the *f*-states of U and the *d*-states of Mo around Fermi level are plotted using bubble diagram, which are shown in Fig. 5 and Fig. 6 for Pmmn phase and P6 phase respectively. There are some zones showing hybridization between *d*-states of Mo atoms and *f*-states of U atoms near the Fermi level. For Pmmn phase, these zones are located near the Γ, Z, Y and U points in Brillouin zone. The overlapping of red cycle (*f*-states of U) and black cycle (*d*-states of Mo) represents the specific orbital hybridization. The zones near the A, K points show a clear hybridization for P6 phase by the overlapping. According to the overlapping size of cycles, the contribution share of *d*-states of Mo atoms and *f*-states of U atoms to the hybridization can be observed easily.

The research of thermodynamic properties of nuclear fuel is a significant and essential part for its future practical applications. The thermodynamic properties of orthorhombic and hexagonal

$U_2Mo$ were investigated employing the PHONOPY code in the present work. Firstly, different sized unit cells were constructed near the equilibrium volume. Then atoms position and cell shape were optimized with fixed volume. In our work, the calculations were performed employing 10 vol points for orthorhombic structure and 8 vol points for hexagonal structure. Force constants were calculated through phonon calculations based on density functional perturbation theory (DFPT) (Baroni et al., 1987, 2001). Within the framework of the quasi-harmonic approximation (QHA) based on 2 × 2 × 2 supercells, the thermal properties of $U_2Mo$ can be calculated from their phonon density of states. Gibbs free energy G (T, p) at given temperature T and pressure p is obtained from the schematic equation as follow:

$$G(T,p) = \min_V \left[U(V) + F_{phonon}(T;V) + pV\right] \quad (3)$$

The relations between the Gibbs free energy and the elevated temperature for these two structures are plotted in Fig. 7. We can see that the Gibbs free energy decreases gradually with increasing temperature. It can also be observed that Gibbs free energy of P6 phase is smaller than the values of Pmmn phase. These results indicate that hexagonal P6 structure is more thermodynamically stable than orthorhombic Pmmn structure (Zhou et al., 2012).

For both phases of $U_2Mo$, the change of free energy with volume at different temperature is illustrated in Fig. 8. The ten curves are the fits to Vinet equation of states (EOS) at temperatures from 0 to 900 K with 100 K step. The minimum values at every temperature are depicted by the cross symbols. The individual lattice parameters for this minimum at different temperatures are listed in Table 3.

Based on these data depicted in Fig. 8, the thermal volume expansion for these two structures can be derived. Thermal volume expansion is defined as $\Delta L/L_0$, where $L_0$ is $L = V^{1/3}$ at 300 K and $\Delta L = L - L_0$. As shown in Fig. 9, the thermal expansion of the volumes increases with temperature for both phases. The results of orthorhombic Pmmn phase is in good agreement with the results by Wang et al. (2014). We provide in Fig. 10, the relations between expansion coefficients $\alpha$ and the temperature T. Fig. 10 shows that $\alpha$ increases exponentially with T at low temperature and gradually approaches a linear behavior at higher temperature for both structures. Furthermore, Fig. 11 presents heat capacity $C_P$ and $C_V$ versus temperature. When T < 150 K, $C_P$ and $C_V$ increase rapidly with $T^3$. At high temperature, heat capacity increases linearly. This indicates that the interactions between U and Mo atoms are much stronger in low temperature region.

## 4. Conclusions

In summary, the mechanical, electronic and thermodynamic properties of hexagonal and orthorhombic $U_2Mo$ compounds were studied by first-principle calculation. Our calculation revealed that the energy of hexagonal structure is 0.0365mRy lower than orthorhombic structure under the equilibrium volume. The calculated elastic constants satisfy the mechanical stability criteria, demonstrating the elastic stability of both structures. The G/B values indicate that hexagonal and orthorhombic $U_2Mo$ are both ductile. The calculated phonon dispersion curves without imaginary phonon mode confirm these two compounds are dynamically stable.

The stress-strain relationships under tensile were studied. The ideal tensile strengths for Pmmn phase are about 18–21 GPa along the <100>, <110>, <111> directions, while hexagonal P6 structure's ideal tensile strengths are 21.2 GPa and 14.6 GPa along the <1010> and <1000> directions, respectively. The stress-strain relations and the corresponding theoretical tensile strengths exhibit strong anisotropy in their selected directions.

Through the analyses of the electrical structures, hybridizations between *d*-states of Mo atoms and *f*-states of U atoms were observed. The thermodynamic properties of $U_2Mo$ such as the Gibbs free energy, heat capacity and linear expansion coefficient were also obtained within the harmonic approximation.

## Acknowledgment

This work was supported by the National Natural Science Foundation of China (Grant No. 11604029), the Open Research Fund of Computational Physics Key Laboratory of Sichuan Province, Yibin University (No. JSWL2014KF02) and by the Project of Science and Technology Department of Sichuan Province (No. 2015JY0167) and China Postdoctoral Science Foundation funded Project (Grant No. 2015M582767XB).

## References

Alonso, P.R., Rubiolo, G.H., 2007. The role of multisite interactions in the formation energy of bcc γ(U,Mo) disordered phase. Modell. Simul. Mater. Sci. Eng. 15, 263–273.
Baroni, S., Giannozzi, P., Testa, A., 1987. Green's-function approach to linear response in solids. Phys. Rev. Lett. 58, 1861–1864.
Baroni, S., De Gironcoli, S., Dal Corso, A., Giannozzi, P., 2001. Phonons and related crystal properties from density-functional perturbation theory. Rev. Mod. Phys. 73, 515–562.
Blöchl, P.E., 1994. Projector augmented-wave method. Phys. Rev. B 50, 17953–17979.
Born, M., Huang, K., 1954. Dynamical Theory of Crystal Lattices. Clarendon press.
Burkes, D.E., Hartmann, T., Prabhakaran, R., Jue, J.-F., 2009. Microstructural characteristics of DU–xMo alloys with x=7–12 wt%. J. Alloys Compd. 479, 140–147.
Burkes, D., Mickum, G., Wachs, D., 2010a. Thermo-physical Properties of U-10Mo Alloy. Technical Report, INL/EXT-10–19373. Idaho National Laboratory.
Burkes, D.E., Papesch, C.A., Maddison, A.P., Hartmann, T., Rice, F.J., 2010b. Thermophysical properties of DU–10 wt.% Mo alloys. J. Nucl. Mater 403, 160–166.
Craik, R.L., Birch, D., Fizzotti, C., Saraceno, F., 1962. Phase equilibria in uranium-rich binary alloys containing molybdenum and zirconium and the effect of ternary additions of carbon. J. Nucl. Mater 6, 13–25.
Dabush, E., Sariel, J., Dahan, I., Kimmel, G., 2002. JCPDS-International Centre for Diffraction data 2002. Adv. X-Ray Anal. 45, 146.
Hill, R., 1952. The elastic behaviour of a crystalline aggregate. Proc. Phys. Soc. Sect. A 65, 349.
Howlett, B.W., 1970. A study of the shear transformations from the gamma-phase in uranium-molybdenum alloys containing 6.0–12.5 at % molybdenum. J. Nucl. Mater 35, 278–292.
Jaroszewicz, S., Losada, E.L., Garcés, J.E., Mosca, H.O., 2013. Ab initio calculation of mechanical and thermal properties of $U_2Mo$ intermetallic. J. Nucl. Mater 441, 119–124.
Kresse, G., Furthmüller, J., 1996a. Efficiency of ab-initio total energy calculations for metals and semiconductors using a plane-wave basis set. Comp. Mater. Sci. 6, 15–50.
Kresse, G., Furthmüller, J., 1996b. Efficient iterative schemes for ab initio total-energy calculations using a plane-wave basis set. Phys. Rev. B 54, 11169–11186.
Kresse, G., Hafner, J., 1993. Ab initio molecular dynamics for liquid metals. Phys. Rev. B 47, 558–561.
Kresse, G., Joubert, D., 1999. From ultrasoft pseudopotentials to the projector augmented-wave method. Phys. Rev. B 59, 1758–1775.
Kutty, T.R.G., Dash, S., Banerjee, J., Kaity, S., Kumar, A., Basak, C.B., 2012. Thermophysical properties of $U_2Mo$ intermetallic. J. Nucl. Mater 420, 193–197.
Landa, A., Söderlind, P., Turchi, P.E.A., 2011. Density-functional study of U–Mo and U–Zr alloys. J. Nucl. Mater 414, 132–137.
Liu, B.Q., Duan, X.X., Sun, G.A., Yang, J.W., Gao, T., 2015. Structural instabilities and mechanical properties of $U_2Mo$ from first principles calculations. PCCP 17, 4089–4095.
Losada, E.L., Garcés, J.E., 2015. Structural instability and ground state of the $U_2Mo$ compound. J. Nucl. Mater 466, 638–645.
Losada, E., Garcés, J., 2016. Ground state of the $U_2Mo$ compound: physical properties of the Ω-phase. J. Nucl. Mater 479, 59–66.
Pedrosa, T.A., dos Santos, A.M.M., Lameiras, F.S., Cetlin, P.R., Ferraz, W.B., 2015. Phase transitions during artificial ageing of segregated as-cast U–Mo alloys. J. Nucl. Mater 457, 100–117.
Perdew, J.P., Burke, K., Ernzerhof, M., 1996. Generalized gradient approximation made simple. Phys. Rev. Lett. 77, 3865–3868.
Pugh, S., 1954. XCII. Relations between the elastic moduli and the plastic properties of polycrystalline pure metals. Lond. Edinb. Dublin Philosophical Mag. J. Sci. 45, 823–843.
Rechtien, J., Nelson, R., 1973. Phase transformations in uranium, plutonium, and neptunium. Metall. Trans. 4, 2755–2765.
Reuss, A., 1929. Berechnung der fließgrenze von mischkristallen auf grund der

plastizitätsbedingung für einkristalle. ZAMM-J. Appl. Math. Mechanics/Zeitschrift für Angewandte Math. und Mech. 9, 49–58.
Rough, F.A., Bauer, A.A., 1958. Constitution of Uranium and Thorium Alloys. Battelle Memorial Institute.
Tangri, K., Williams, G., 1961. Metastable phases in the uranium molybdenum system and their origin. J. Nucl. Mater 4, 226–233.
Togo, A., Oba, F., Tanaka, I., 2008. First-principles calculations of the ferroelastic transition between rutile-type and $CaCl_2$-type $SiO_2$ at high pressures. Phys. Rev. B 78, 134106.
Togo, A., Chaput, L., Tanaka, I., Hug, G., 2010. First-principles phonon calculations of thermal expansion in $Ti_3SiC_2$, $Ti_3AlC_2$, and $Ti_3GeC_2$. Phys. Rev. B 81, 174301.
Tupper, C.N., Brown, D.W., Field, R.D., Sisneros, T.A., Clausen, B., 2012. Large strain deformation in uranium 6 Wt Pct Niobium. Metall. Mater. Trans. A 43, 520–530.
Van Thyne, R., McPherson, D., 1957. Transformation kinetics of uranium-molybdenum alloys. Trans. ASM 49, 598–621.
Voigt, W., 1928. In: Teubner, B.G., Edwards, J.W. (Eds.), Lehrbuch der Kristallphysik (mit Ausschluss der Kristalloptik). Leipzig Berlin. Ann Arbor, Mich.
Wang, X., Cheng, X., Zhang, Y., Li, R., Xing, W., Zhang, P., Chen, X.-Q., 2014. First-principles study of ground-state properties of $U_2Mo$. PCCP 16, 26974–26982.
Zhang, R., Sheng, S., Veprek, S., 2007. First principles studies of ideal strength and bonding nature of AlN polymorphs in comparison to TiN. Appl. Phys. Lett. 91, 031906.
Zhou, D., Liu, J., Xu, S., Peng, P., 2012. Thermal stability and elastic properties of $Mg_2X$ (X= Si, Ge, Sn, Pb) phases from first-principle calculations. Comp. Mater. Sci. 51, 409–414.